Railway Track Performance Monitoring and Safety Warning System

Chung-Yue Wang[1]; Hsin-Chu Tsai[2]; Chi-Shian Chen[3]; and Hao-Lin Wang[4]

Abstract: To install the continuous welded rail (CWR) on the viaduct, it is necessary to consider the accumulated axial force owing to temperature difference and the additional force of the rail exerted by the track-bridge expansion as a result of temperature difference, the so-called track–bridge interaction. This paper used *A*-thermal fiber bragg grating (FBG) sensors which do not need the temperature compensation, and electronic sensors as monitoring instruments to detect performance changes in CWR axial force. These optical fiber sensors coupled with the developed track axial force calculation software and monitoring platforms calculate the axial force distribution along the track to be monitored. To better understand the influence of the change in the bridge's structure expansion and the change in concrete slab strain on track axial forces, sensors are set up at bridge expansion joints (EJs), rail ends, and concrete slab beds. Monitoring results show that optic fiber sensors provide sensitive, clear, and stable signals. They are also durable and appropriate for long-term monitoring, providing a complete track safety warning system. **DOI: 10.1061/(ASCE)CF.1943-5509.0000186.**

CE Database subject headings: Railroad tracks; Thermal stress; Fiber optics; Monitoring; Safety.

Author keywords: Railroad tracks; Thermal stress; Fiber optics; Monitoring.

Introduction

A well-known risk with continuous welded rail (CWR) is its potential for buckling owing to high thermally induced compressive loads, with possible train derailment consequences. When ambient temperature is high, rail temperature rises as well. Because the thermal expansion of the rail is constrained, this temperature increase results in large compressive forces in the rail, which can cause the track to buckle laterally (Kish and Samavedam 1991).

When installing CWR on bridges, the rail bears additional stress caused by factors such as the additional force produced by the deformation of the bridge structure as trains pass through, the expansion of bridges caused by the temperature change, and the longitudinal forces generated by train braking. The mutual influence between rails and bridges is known as the track–structure interaction (Reis et al. 2007). Usual track buckling is caused by the additional axial stress owing to the thermally induced expansion of the bridge. As the bridge and rail expand because of temperature changes differently, a greater amount of rail longitudinal internal force is generated at the free-end expansion joints (EJs) on the bridge owing to the huge amounts of accumulated rail axial force and the additional longitudinal force produced by the bridge. This increases the potential for rail buckling that leads to derailment (Matsumoto and Asanuma 2007). Derailment happens because the railway transport system often travels at high speed and is heavily loaded with passengers, and it can result in heavy casualties and traffic disruption; substantial economic compensation is also paid. Monitoring systems can help prevent derailments owing to buckling by monitoring constantly the internal force distributions of CWR and the maximum axial stress accumulation. After receiving the warning signal, rail axial pressure can be reduced before buckling or limiting the speed of trains.

Traditional methods for monitoring rail axial force consist of destructive and nondestructive methods (Kish and Coltman 1990). The simplest, but destructive method, is cutting the rail and measuring the rail ends displacements. Using this technique, one can determine the approximate value of stress in the rail before it was cut. Rail lift up is considered a partially destructive measurement. This method must first unleash 30 m of rail fasteners to calculate the axial force, and the rails are then pulled upward until the rail is vertically displaced to reach 100 mm of deformation. The rail axial stress can be calculated using the imposed force and rail temperature. Szelazek (1998) used ultrasonic stress measurement to monitor the temperature stress on CWR, on the basis of the elastoacoustic effect. Rail stress can be estimated by observing the changes in ultrasonic velocity with different stresses. Lo et al. (2004) showed magnetic measurements can be used to detect nondestructively the stress concentrations in magnetic materials. A prototype unit has been developed to apply this technique to rail (Wegner, 2005). This technique measures the rail stress and neutral temperature by using the Barkhausen noise method which utilizes the relationship between the level of Magnetic Barkhausen noise and the stress in a ferrous material. Damljanovic and Weaver (2005) used laser vibrometry technique and conducted laboratory tests to infer the axial stress in 136RE rail by vibrating the sample laterally. Damljanovic concluded that longitudinal force affects the wavelength of bending waves and that the wavelengths can

[1]Professor, Dept. of Civil Engineering, National Central Univ., No. 300, Zhongda Rd., Zhongli City, Taoyuan County 320, Taiwan. E-mail: cywang@cc.ncu.edu.tw

[2]Ph.D. Candidate, Dept. of Civil Engineering, National Central Univ., No. 300, Zhongda Rd., Zhongli City, Taoyuan County 320, Taiwan (corresponding author). E-mail: 943402022@cc.ncu.edu.tw

[3]Ph.D. Candidate, Dept. of Civil Engineering, National Central Univ., No. 300, Zhongda Rd., Zhongli City, Taoyuan County 320, Taiwan. E-mail: s1322006@cc.ncu.edu.tw

[4]Ph.D. Candidate, Dept. of Civil Engineering, National Central Univ., No. 300, Zhongda Rd., Zhongli City, Taoyuan County 320, Taiwan. E-mail: s1342022@cc.ncu.edu.tw

Note. This manuscript was submitted on April 6, 2010; approved on October 19, 2010; published online on October 21, 2010. Discussion period open until May 1, 2012; separate discussions must be submitted for individual papers. This paper is part of the ***Journal of Performance of Constructed Facilities***, Vol. 25, No. 6, December 1, 2011. ©ASCE, ISSN 0887-3828/2011/6-577–586/$25.00.

be inferred by comparing the vibration amplitude distributions with distributions on the basis of the wavenumbers obtained from elastic waveguide theory. But this technique required a high precision finite element analysis for the prediction of wavenumbers and an elaborate fitting procedure to the bending modes.

Even though most methods described in the preceding text can effectively measure rail axial stress, the process nevertheless hinders traffic, charges a lot of time, and needs maintenance, and the measured axial stress only responds to the structure in a single area. Manual measurements and monitoring are performed on a regular basis, so that rail response and security conditions cannot be reflected in real-time and an emergency warning system cannot be implemented immediately. Although the electric resistance wire strain gauge could resolve this problem, its long-distance distribution causes too much noise in signal transmissions. Moreover, the gauge has poor durability and is severely interfered with by the electromagnetic waves in the railway system. These factors, coupled with the impact of adverse circumstances on the rail site, always cause the system to fail (Tam and Ho 2007).

Therefore, the real-time safety monitoring system, appropriate for the rails without hampering traffic, must be able to monitor long range of rail and to guard the sensor from electromagnetic waves interference from the railway system. The optical fiber sensing method is not invited to the interference of electromagnetic waves and can be distributed over long distances for the railway health monitoring (Wang et al. 2005). This paper applies *A*-thermal fiber bragg grating (FBG) sensors for the full-time monitoring of track systems. Moreover, when CWR are laid on a bridge, an additional longitudinal force will be exerted on the welded rail owing to the amount of thermal expansion. Through the monitoring system, this study also observes bridge–rail interaction behavior and proposes an effective track safety warning mechanism.

Structure of the Track Performance Monitoring System

This section explains how the traditional electronic sensors and FBG sensors are combined and then installed at appropriate positions to measure the real-time changes of strain, temperature, and displacement of the CWR and the concrete slab rail bed. The bridge–rail interaction behavior, the longitudinal force distribution of the rail, and the maximum rail axial force were observed. With the proposed safety monitoring platform, this monitoring system can provide real-time monitoring and safety warning.

Fiber Bragg Grating Sensor

A CWR is a welded rail longer than 200 m with movable and immovable sections. The rail in the movable section compresses as induced by thermal changes, but the immovable section transfers the compression into rail internal force, that is, the rail axial force, which is accumulated from the rail end at EJ to the immovable section. The rail axial force in the immovable section cannot be obtained using direct measurement of the rail strain, but the actual accumulative axial force can be estimated by measuring the strain differences in the free ends and in the immovable section. The rail axial force on the viaduct is not a smooth straight line, but is undulating as it is affected by the allocation of the bridge span and the support.

Thus, from the rail end to the immovable section, 132 FBG sensors were installed on 44 sections along the rail. The total length of the monitoring region was 227 m, distributed on two four-span continuous bridges, as shown in Fig. 1. First, two anchor plates were welded to the web of the rails, and then the FBG sensors were installed and exerted with some pretension (Fig. 2). To prevent the impact by the ballast and the environmental effect such as humidity, thermal stretching of the cable, and ultraviolet, a plastic casing (Fig. 3) is used. Another 10 FBG sensors were installed on the concrete slabs close to the track to monitor their responses. An eight-channel interrogator is used to acquire the data of 142 FBG sensors.

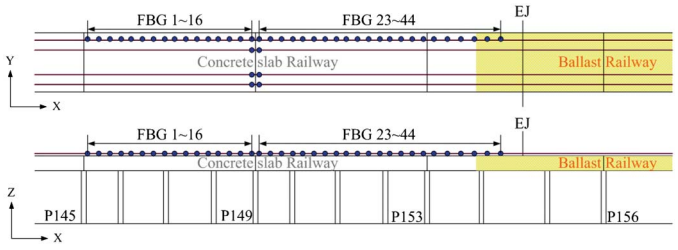

Fig. 1. Configuration of FBG sensors

Electronic Types of Sensor

To observe the changes of the bridge EJ against the rail end and the long-term variation trends with temperature, the monitoring system use three kinds of electronic sensors. Thermal couples are installed to measure the temperatures of the air, track, and concrete. Extensometer is used to measure the displacement of the free end of the track at the EJ (Fig. 4). Whereas, the variation of the gap distance of the EJ of the concrete bridge is measured by the linear variable differential transformer (LVDT) (Fig. 5).

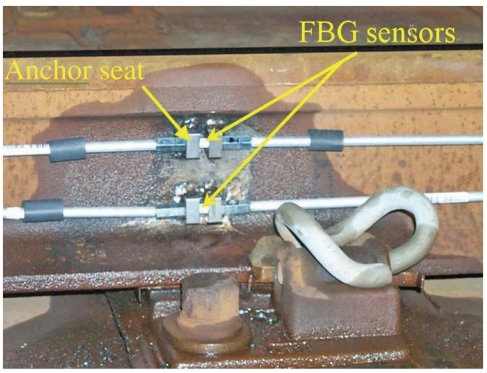

Fig. 2. FBG sensor installed on the track (photo by the authors)

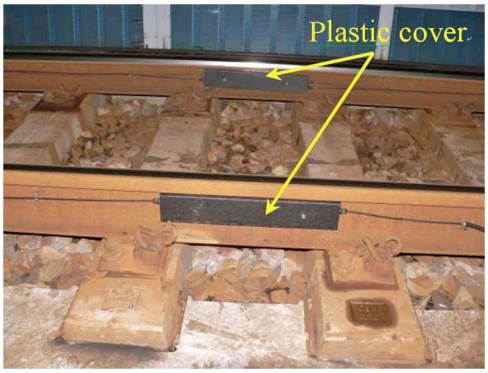

Fig. 3. FBG sensor is protected by a plastic casing from environmental impacts (photo by the authors)

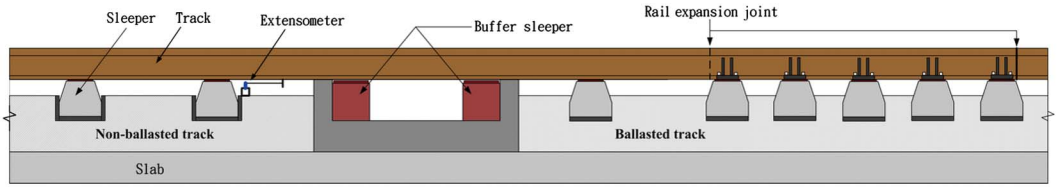

Fig. 4. Measurement of the displacement of track EJ using an extensometer

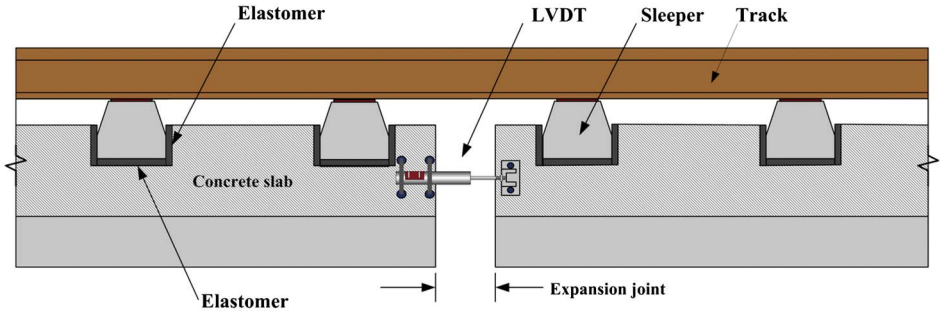

Fig. 5. Measurement of the displacement of bridge EJ using LVDT

Monitoring Platform

A structural condition monitoring platform is developed to acquire, analyze, and manage the data from sensors. Through the asymmetric digital subscriber line (ADSL) and internet system, the performance of these sensing data can be studied at any place of the world. User can generate reports from the data stored in the management system and manager can inspect whether sensors are under control or not. Once the signals trigger the warning criteria, messages will be sent to the authorized agencies and engineers by fax, e-mail, and mobile phone.

Backward Analysis of Internal Forces of Rail Track

Railway track is subjected to vertical, lateral, and longitudinal forces from the environment, traffic, and maintenance, which the track-structure must safely resist. When the longitudinal rail force is not adequately constrained by the lateral resistance of the track, a track buckle can occur (Sussmann et al. 2003). From the fundamentals of track buckling, it is seen that the real-time monitoring of the longitudinal strains and temperature of track at some critical points can assist engineers to conduct the safety diagnosis and provide the warning signal of track buckling.

According to the three-dimensional beam theory, the axial strains of points in a cross-section of track as shown in Fig. 6, under the action of external loading have the following relations shown in Eq. (1) with the sectional internal forces.

$$\begin{aligned}\varepsilon_1 &= \frac{N_x}{EA} + \frac{M_y}{EI_y}d_1 - \frac{M_z}{EI_z}d_5 + \beta\Delta T \\ \varepsilon_2 &= \frac{N_x}{EA} - \frac{M_y}{EI_y}d_2 - \frac{M_z}{EI_z}d_3 + \beta\Delta T \\ \varepsilon_3 &= \frac{N_x}{EA} + \frac{M_y}{EI_y}d_1 + \frac{M_z}{EI_z}d_4 + \beta\Delta T\end{aligned} \tag{1}$$

where N_x = the internal axial force; M_y, M_z = the internal bending moments related to y and z axes, respectively; β = the thermal expansion coefficient; ΔT = the temperature change from the neutral temperature (the temperature at which the net longitudinal force in the rail is zero); I_y and I_z = the mass moment of inertias of the y and z axes, respectively; ε_i ($i = 1, 3$) = axial strains to be measured; d_i ($i = 1, 5$) = the distances from gauges to the corresponding coordinate axes. Once the temperature change ΔT and the three axial strains ε_1, ε_2, ε_3 are measured, the internal forces (N_x, M_y, M_z) and the curvatures (k_y, k_z) of the track cross-section can be calculated by using Eqs. (2) and (3).

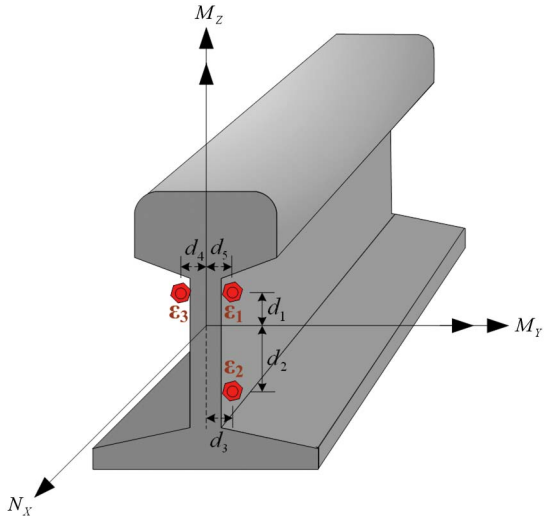

Fig. 6. Arrangement of strains sensors at a cross-section of track

$$\begin{Bmatrix} N_x \\ M_y \\ M_z \end{Bmatrix} = \begin{bmatrix} \frac{1}{EA} & \frac{d_1}{EI_y} & \frac{-d_5}{EI_z} \\ \frac{1}{EA} & \frac{d_2}{EI_y} & \frac{-d_3}{EI_z} \\ \frac{1}{EA} & \frac{d_1}{EI_y} & \frac{d_4}{EI_z} \end{bmatrix}^{-1} \begin{Bmatrix} \varepsilon_1 - \beta\Delta T \\ \varepsilon_2 - \beta\Delta T \\ \varepsilon_3 - \beta\Delta T \end{Bmatrix} \tag{2}$$

$$\kappa_y = \frac{(\varepsilon_1 - \varepsilon_2)}{(d_1 + d_2)} \qquad \kappa_z = \frac{(\varepsilon_1 - \varepsilon_3)}{(d_4 + d_5)} \tag{3}$$

Data Analysis

Analysis of Temperature Changes

Fig. 7 presents the temperature histories of the air, rail, and concrete during one day. The rail temperature is higher than the air temperature by 10–15°C in the hot summer. Because concrete has low thermal conductivity, it shows a time delay in its temperature change trends compared to the air temperature. The range of rail temperature variation can be clearly understood through the long-term observation of the temperature data. Fig. 8 presents the rail temperature monitoring data distribution from February to June, and Fig. 9 shows the probability density function of rail temperature that provides references for the future installation temperature.

Displacement of the Rail EJ

Fig. 10 shows the rail temperature history and the rail expansion over 1 day. The graph shows that the CWR expands approximately 6.8 mm when the rail temperature changes approximately 20°C. From this expansion amount and rail temperature, an expansion-temperature change figure can be constructed as shown in Fig. 11. Using the linear regression slope of the range of EJ, the expansion of CWR at different temperatures and, the average longitudinal resistance r of the rail exerted by the fastener can be calculated as 3.74 kg/m by using Eq. (4) (Chang 2004). This resistance is relatively low compared to the initial design value of 5.6 kg/m and may result in more rail expansion than allowed by the EJ. However, the additional force caused by the track–bridge interaction can be mitigated.

$$r = \frac{EA\beta^2 T_0}{2a} \qquad T_0 = \frac{T_1 + T_2}{2} \tag{4}$$

where T_1, T_2 = the maximum and minimum rail temperatures, respectively, a = the slope value of the linear regression of the CWR joint expansion figure, β = the coefficient of rail thermal expansion ($\beta = 11.4 \times 10^{-6}(1/°C)$), A = the cross-section area of the rail ($A = 76.86\ cm^2$), E = Young's modulus of elasticity ($E = 2.1 \times 10^6\ kgf/cm^2$)

Fig. 12 compares the displacement of the bridge EJ against the changes in temperature over 1 day. Because the temperature is larger than the installed temperature, the gap of bridge EJ is smaller and the displacement is negative. the change in air temperature is around 10°C and the concrete temperature change is around 3°C, the EJ displacement is 1.17 mm. Long-term observation shows that when the air temperature difference is approximately 20°C, the displacements of joints at two spots of the rail are around 2.3 and 1.25 mm, respectively. Because the structure of the rail contains elastic rubber material elastomer between the sleeper and the concrete slab as shown in Fig. 5, a small amount of displacement (2.3 and 1.25 mm) can be absorbed by the elastic rubber material. Thus, the additional effect of the EJ displacement as a result of temperature changes in the rail is not significant.

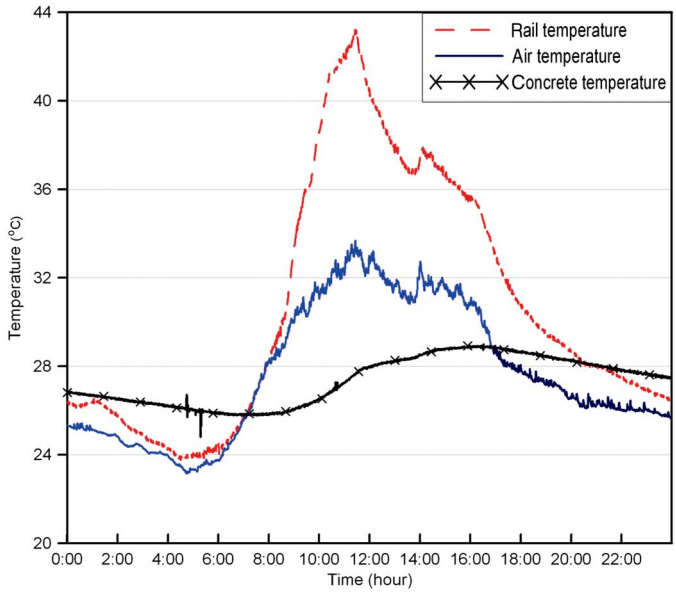

Fig. 7. Difference of temperatures at track and concrete under the same air temperature

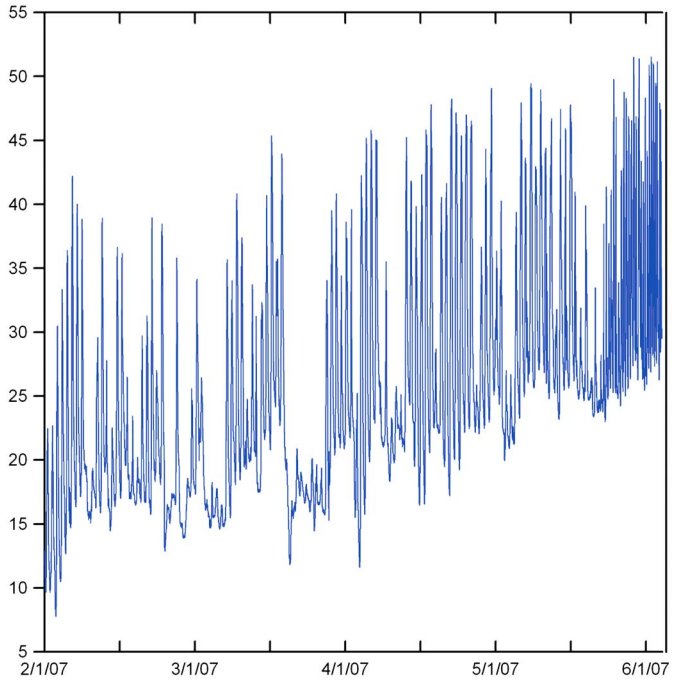

Fig. 8. Temperature variation of rail track within 4 months (February to June, 2007)

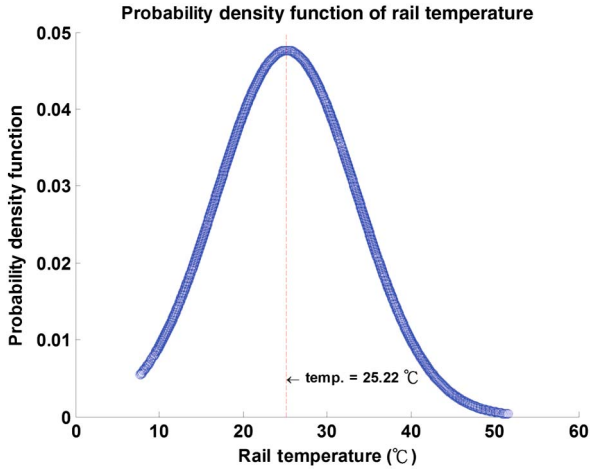

Fig. 9. Probability density function of rail temperature from February to June

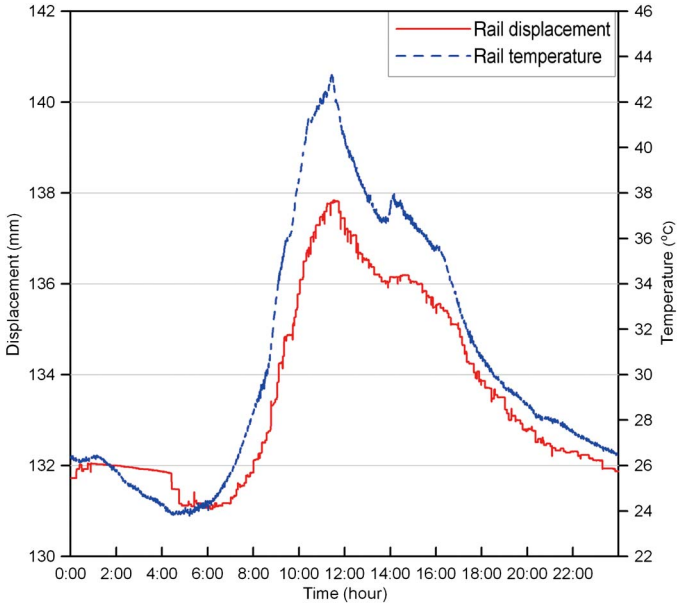

Fig. 10. Joint expansion of CWR at various temperature

Analysis of the Strains of the Rail and the Bridge Deck

The rail strain is the most direct indicator of any abnormal conditions or rail buckling. This is especially true for rails in an immovable section, as they have quite small changes in the strain. Once rail buckling or irregular deformation occurs, a much larger rail strain than usual will also be generated. In addition, the curvature of the cross-section can be calculated using the three strain gauges installed at the rail cross-section and Eq. (3) determines if the rails are laterally or vertically deformed. Fig. 13 compares the performance curve of the rail strain to temperature changes detected by the FBG sensors installed at the track web, indicating that the changes in rail strains and in rail temperature are very similar. Fig. 14 presents the relative curvature of rail cross-section at a distance of 5 m from the EJ with respect to a rail temperature of 30°C. This figure shows that the relative curvature κ_z is significantly greater than κ_y. When there is a 1°C increase in the rail temperature, the curve variations of κ_z and κ_y are respectively 1.275×10^{-6} $(1/\text{cm})$ and 6.828×10^{-7} $(1/\text{cm})$, which, when converted into the relative strains of the two sensors, are respectively 4.78 and 2.73 μstrain.

Fig. 15 compares the strain of a concrete slab to temperature changes. Through long-term monitoring, the strain measured by each strain gauge on this bridge span shows that concrete slab's strain variation is not high. A 1°C increase in the air temperature averagely results in a 5.17 μ strain. Thus, the small quantities of both the monitored strain and the displacement of the bridge EJ, as well as the design of the bridge structure, indicate that the effect of bridge expansion as a result of temperature changes on the rail additional axial force is not significant on this monitored bridge.

Analysis of the Relative Rail Axial Force and Bending Moments

High axial compression stress on the CWR is a major factor in rail buckling. The accumulated axial force of a CWR can be calculated by using Eq. (2), and the rail strain is measured in the immovable section (ε_1, ε_2, ε_3) and at EJ ($\beta\Delta T$). After installing the FBG sensors, the rail fasteners were not released to obtain the strain values of no axial force owing to the restriction of no interruption of operation. Therefore, the strain value at 30°C is used as the initial strain of no axial force. Fig. 16 presents that the values of axial force derived from calculations of the subsequent monitored data are primarily on the basis of relative axial force, which is the relative axial force of the CWR in the immovable section. Fig. 17 shows the internal moment of CWR with respect to the rail temperature.

The relative rail axial force change, bending moment change, and temperature change are similar. To investigate the longitudinal rail axial force distribution from the immovable section to the EJ, we calculated the longitudinally distributed axial force by using the strain data at different rail temperatures with reference to a rail temperature of 30°C. Fig. 18 shows the longitudinal distribution of the relative rail axial force at a rail temperature of 51°C. This figure shows that the greatest value of rail axial force is between sensors 25 and 1 and diminishes toward the movable section when the rail temperature increases, which corresponds to the trends where the axial force of the CWR increases from the movable section to the immovable section owing to the longitudinal resistance of the fastener, thereby confirming that the axial force of the CWR accumulates owing to the buckle grip. The distribution of the CWR shows the boundary between movable and immovable

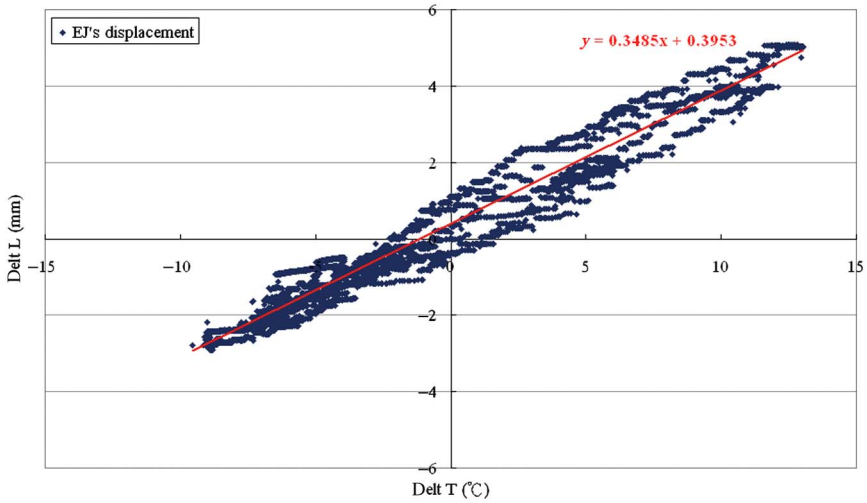

Fig. 11. Longitudinal resistance assessment of CWR EJ, reference track temperature 30°C

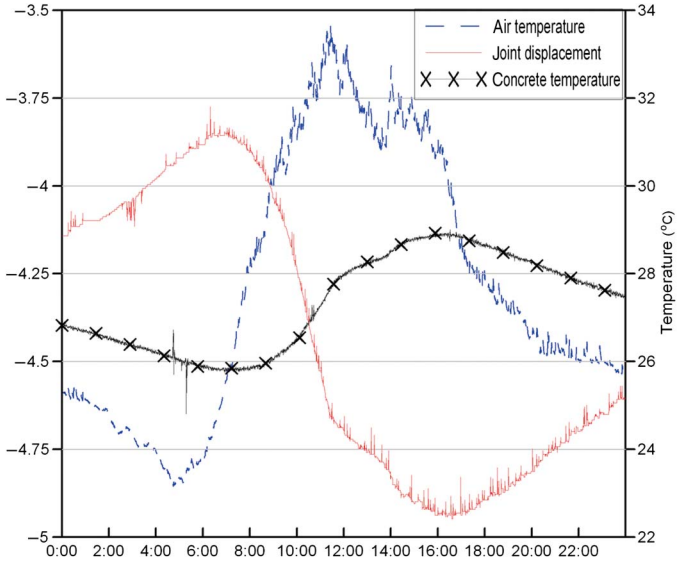

Fig. 12. Variation of the gap of the bridge EJ with respect to temperature of concrete

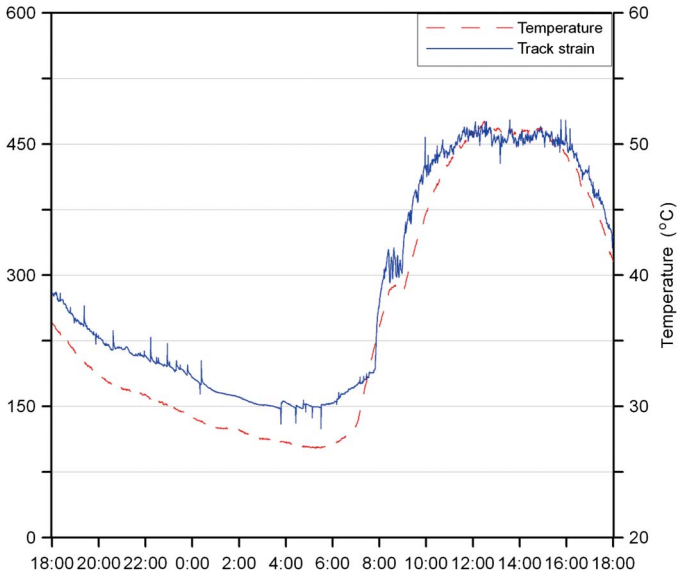

Fig. 13. Variation of track axial strain with respect to track temperature

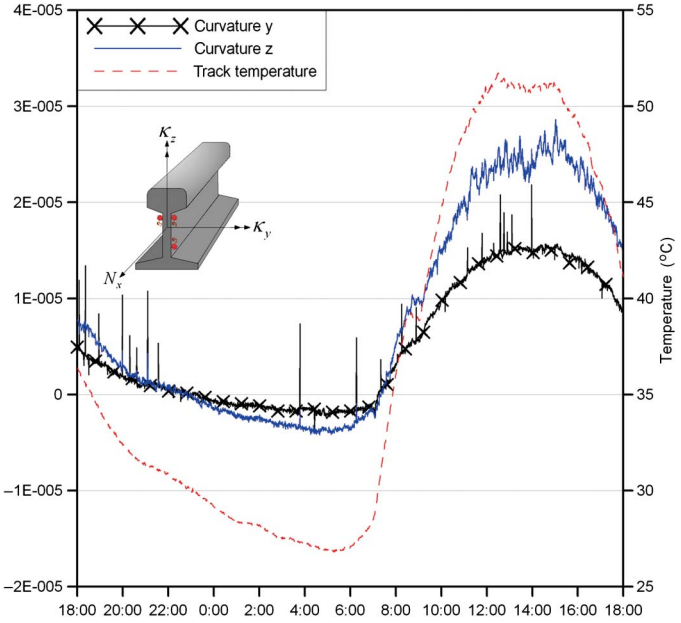

Fig. 14. Relative curvature of track section with respect to the track temperature, reference track temperature 30°C

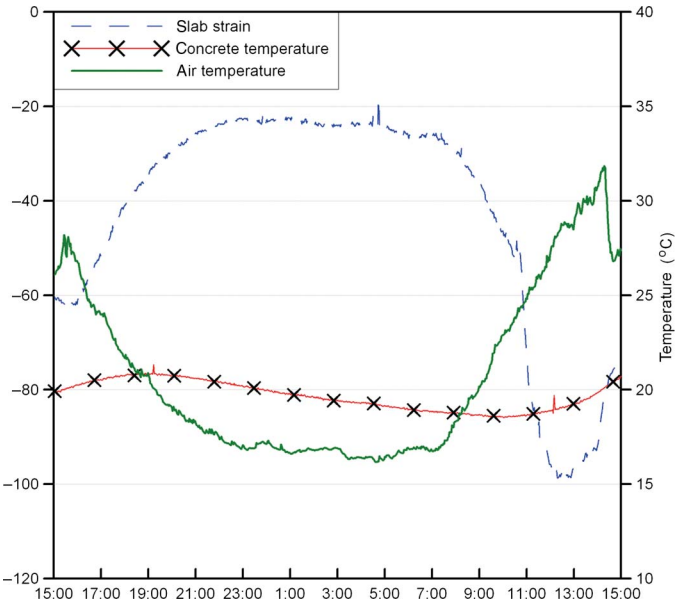

Fig. 15. The curve of the concrete slab strain with respect to the concrete and air temperatures

sections, which is at around sensor 26, approximately 107 m away from the rail ends, and is the boundary for the movable section.

On the basis of the relative axial force distribution and relative rail temperature, it can be calculated that in the immovable section, a 1°C rise in the rail temperature increases averagely the rail relative axial force by 2.38 tons. Because the track–bridge interaction is not significant, the calculated relative axial force in this monitoring system is slightly higher than the axial force of 1.84 tons at the temperature difference of 1°C derived by using Eq. (5), which calculates the temperature stress of ordinary railroads at road embankment sections.

$$P_t = EA\beta\Delta T \tag{5}$$

Rail Safety Warning System

The rail safety warning system is fully automatic, including data acquiring, analyzing, interpreting, and signaling. These tasks are performed by computers in the control center. Whenever a monitored value exceeds the alarm level or if there are abnormalities, the monitoring system will automatically send out text messages and e-mails to relevant operators, who will immediately take necessary actions. Therefore, this research must determine in advance the alarm value and action value of each parameter of the warning system. The alarm value can be established by using the requirements in the specification or by the predefined track-structure system parameters, the rail installation temperature, the ballast lateral resistance and lateral alignment to analyze criticality and evaluate safety of the CWR (Kish and Samavedam 1999). By evaluating the rail buckling probability and rail temperature or other parameter relationships, we can further understand the cut-off of each parameter when buckling occurs.

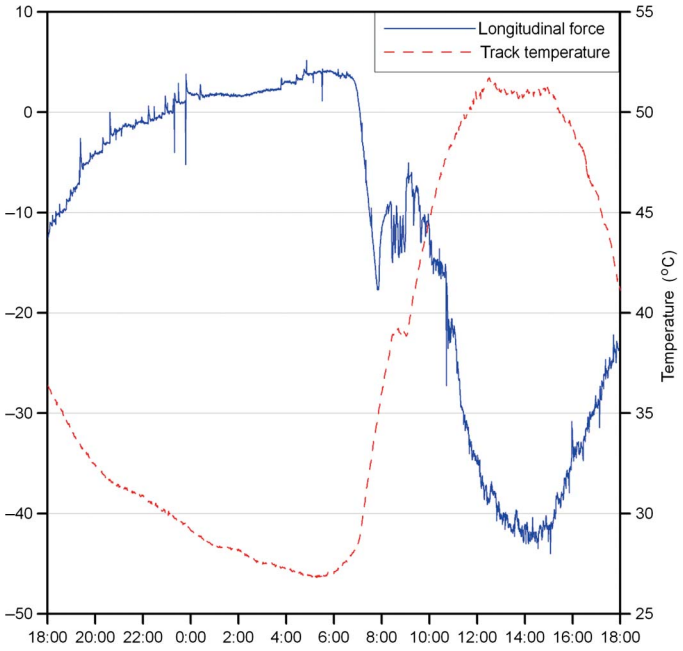

Fig. 16. Relative axial force of CWR with respect to the track temperature, reference track temperature 30°C

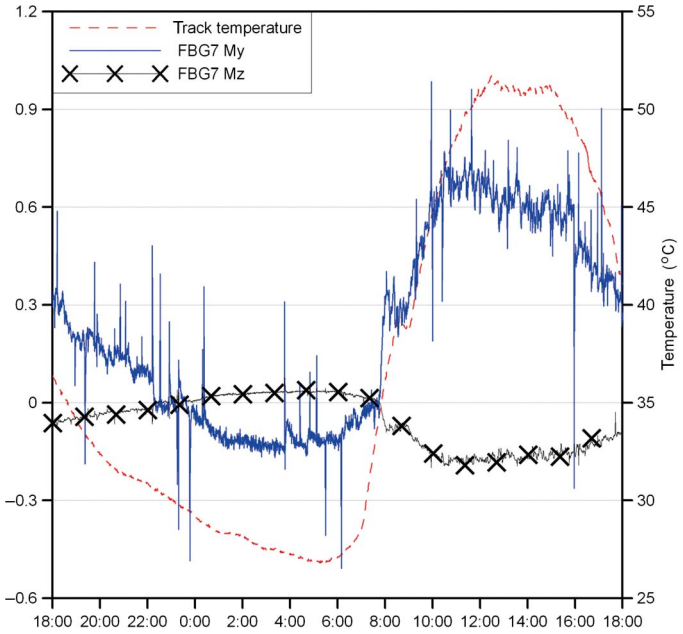

Fig. 17. Relative moment of CWR at the section FBG 7 with respect to the track temperature, reference track temperature 30°C

The alarm value can also be established by using a regression curve on the basis of the long-term motoring data. Different alarm values with different aspects can be built using the displacement of rail lateral deformation, the curvature of the rail cross-section, the rail end expansion, and the rail temperature, which are commonly seen. This research planned to set up the action value and the alarm value for rail temperature on the basis of the calculation equation of the rail temperature stress and the rail buckling strength theory. In addition, on the basis of the rail end expansion figure graphed using the long-term monitoring data and its standard deviation, this study calculates the regression curves of the alarm and action values to serve as a basis for the rail safety monitoring warning system.

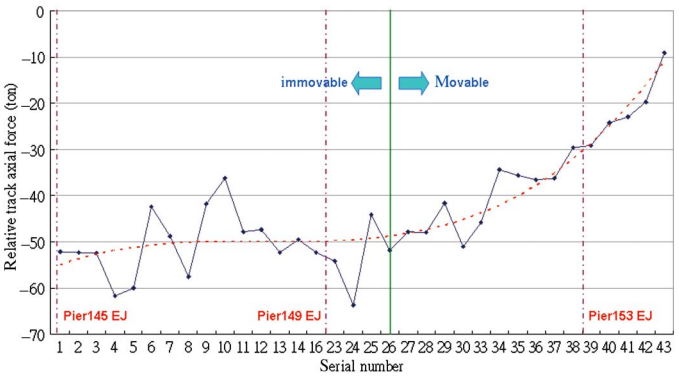

Fig. 18. Longitudinal distribution of the rail relative axial force

Developing Rail Temperature Alarm Values

The rail axial force, the rail expansion displacement, the additional influence of the bridge on the rail, and the buckling potential energy are directly related to the rail temperature. Thus, monitoring rail temperature can directly reflect the abnormalities of systems and potential disasters. Moreover, this approach is practical because it is easy to operate and is economical. This study calculated the greatest axial force under the highest rail temperature and the buckling strength of the monitored rail on the basis of the initially designed basic data combined with partial monitoring statistics parameters. The alarm value can be set by calculating the rail temperature at which rail buckling occurs by using the equation that calculates the maximum rail axial force and the buckling strength.

The monitored railroad bridge is curved, with a minimum curvature radius $R = 410$ m, installation temperature of 30°C, rail lateral moment of inertia $J = 512.9$ cm^4, railway bedding longitudinal resistance $r = 3.74$ kg/cm (value calculated from monitoring data), and railway bedding horizontal resistance $g = 6.5$ kg/cm. Introducing these parameters in to Eq. (6) derived by the Japanese National Railways, using the minimum energy principle to calculate the minimum buckling strength $P_{t,\min}$, which is also called the rail buckling strength P_{cr} (Sato 2001) between the buckling strength P_t and the balanced axial force P, a value of 88.46 tf can be obtained as shown in Fig. 19.

$$P_t = P + \sqrt{\frac{\gamma^2 r^2}{P} + \frac{\alpha r}{P^3\sqrt{P}}\left\{\left(g - \xi\frac{P}{R}\right)^2 + K\left(g - \xi\frac{P}{R}\right)\frac{P}{R}\right\}} - \frac{\gamma r}{\sqrt{P}} \tag{6}$$

where P_t = the rail axial force before buckling instant (kgf), P = the balanced axial force after buckling instant (kgf), n = number of buckling waves, $\mu = 8.8857$, $\varphi = 817.7714$, $\xi = 1$

$$\gamma = \frac{(n+1)\sqrt{2\pi\sqrt{EJ}}}{2} = 145811 \tag{7}$$

$$\alpha = 8\mu E^2 JA\sqrt{EJ} = 4.06 \times 10^{23} \tag{8}$$

$$K = \frac{\varphi}{2\mu} = 1.0 \tag{9}$$

$P_{cr} = P_{t,\min} = 88.46$ tf, when $P = 58.9$ tf

By using Eq. (10), we can further calculate the rail temperature at which buckling occurs on the basis of the rail buckling strength.

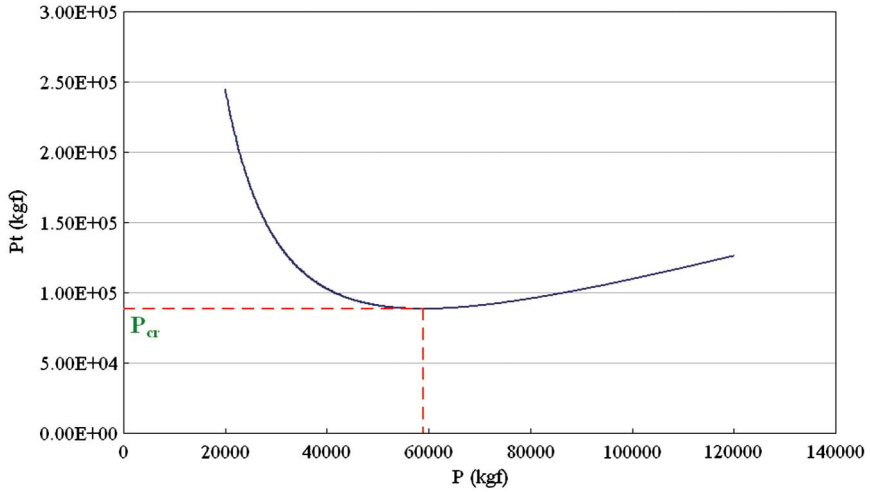

Fig. 19. The diagram of the rail buckling strength and the balanced axial force after buckling

$$P_{cr} = P_t + \frac{1}{2}r\ell = EA\beta\Delta T + \frac{1}{2}r\ell \le \frac{P_{cr}}{F.S.} = \frac{88.46}{1.25} = 70.77 \text{ tf} \tag{10}$$

where $F.S.$ = safety factor, and ℓ = length of the bridge span (m).

Although no obvious track–bridge interaction was observed in this monitoring process, during the period of establishing the alarm value of the rail temperature, the additional axial force of the rail exerted by the bridge and the safety factor $F.S. = 1.25$ were considered. After calculation, $\Delta T = 35.4$℃ was obtained. Hence, the rail axial force reaches buckling strength when the rail temperature reaches 65.4℃ ($T = 30 + \Delta T$). The monitoring data of the rail temperature also shows that the average maximum rail temperature was 55℃. Accordingly, the alarm and action values in this warning system were temporarily set at 90% and 95% of the buckling temperatures (65.4℃), which were 58.8℃ and 62.1℃, respectively.

Alarm Values of the Rail Expansion Displacement and the Curvature of the Rail Cross-Section

The installation of CWR on the bridge must take into consideration the rail expansion in terms of maintenance. The EJs at the two ends of the bridge are especially important in terms of the repeated expansion of the CWR. Fig. 20 presents the rail expansion diagram of normal states set by this monitoring system which measured around 25,000 pieces of rail temperature and expansion displacement data from February to April. Rail expansions may dwell in a fixed range of variation under a specific temperature difference except in cases of rail creeping and abnormalities. By using the characteristics of the rail and long-term monitoring data, the upper and lower limits of alarm and action values are calculated as the average expansion plus and minus three times the standard deviation (3σ) and five times the standard deviation, respectively. If there are abnormal expansions, they might be owing to the shortage of the buckle grip of the fastener and the railway bedding longitudinal resistance. Once a large quantity of creeping or expansion occurs, which cannot be dealt with using the EJs, the CWR must be reinstalled.

The curvature of the rail cross-section and average strain are the primary references of this warning system. For healthy tracks and rail systems, cross-section curvatures should dwell in a fixed variation range as the temperature changes, as shown in Figs. 21 and 22, where the relative curvatures κ_y and κ_z of the rail cross-section near the EJ and the temperature difference are shown. Fig. 23 presents a

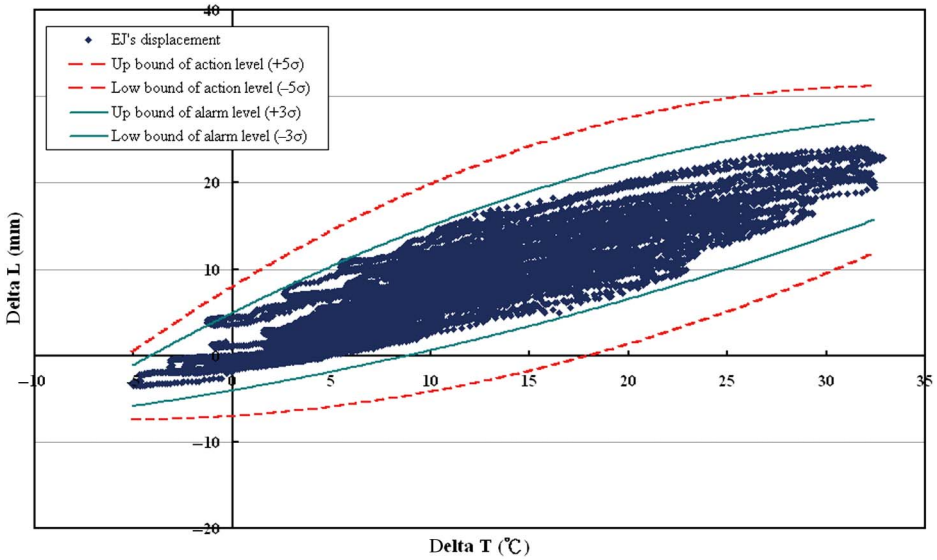

Fig. 20. Rail expansion safety warning figure

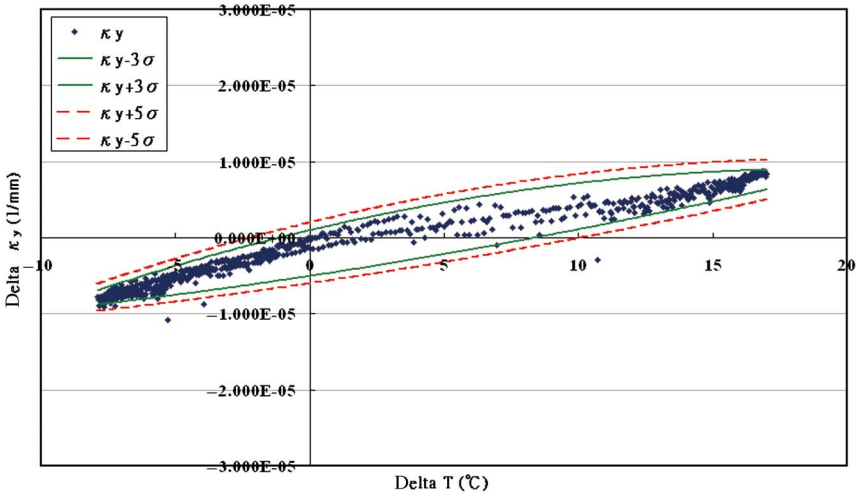

Fig. 21. The curvature κ_y of the rail cross-section safety warning figure

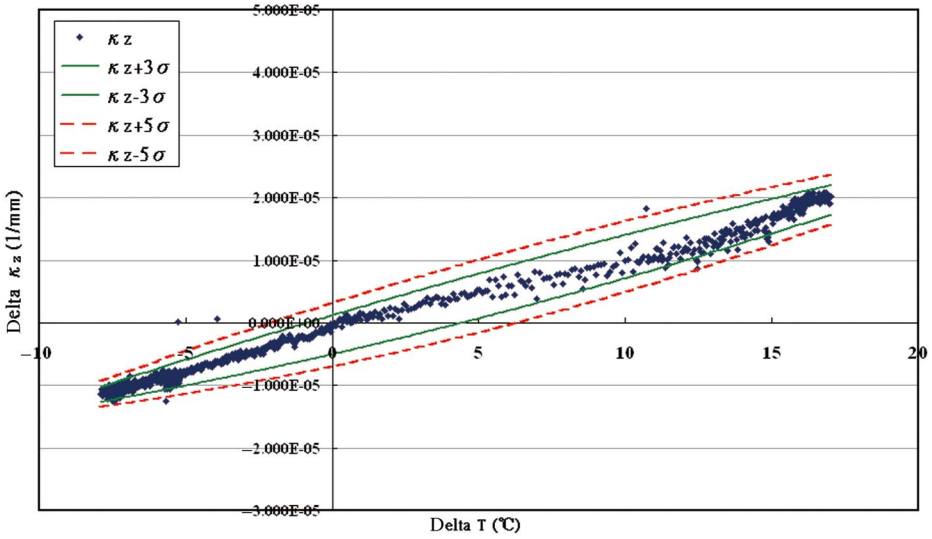

Fig. 22. The curvature κ_z of the rail cross-section safety warning figure

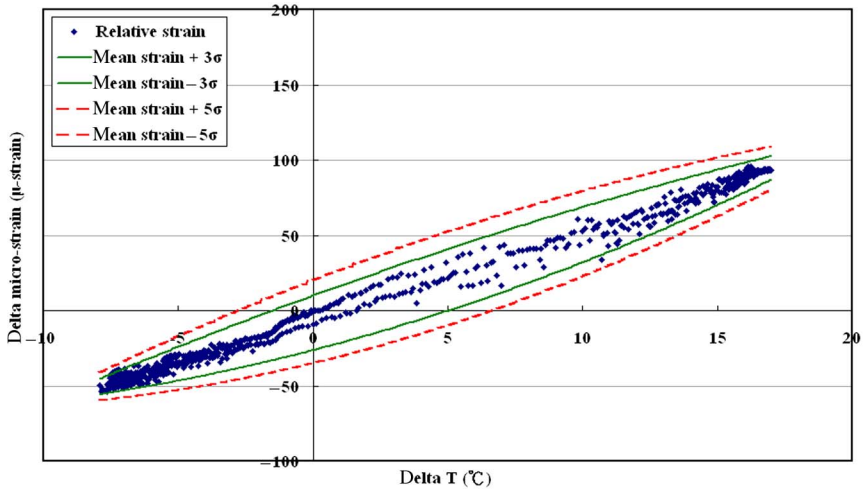

Fig. 23. The average strain of the rail cross-section safety warning figure

diagram of the average strain of the rail cross-section and the temperature difference. After long-term monitoring, a safety range can be established that provides the railway managing unit with the health status of the rails and perform maintenance operations if there are any problems.

Conclusions

This research used *A*-thermal FBG sensors to develop a real-time track monitoring system that is unlike traditional inspection techniques, which must be operated manually on a regular basis. The proposed system can record long-term data on the changes in the rail as the season and temperature changes, providing complete and accurate data. This monitoring system can be placed at important cross-sections or at places near constructions, so that when the system senses an abnormality, it can send out a warning to prevent serious casualties. Some preliminary results obtained from the field measurement over a certain period in collaboration with Taiwan Railway Reconstruction Bureau (TRRB) are presented. The field measurement results demonstrated that the FBG sensors integrated with some conventional sensors can effectively monitor the track–bridge interaction behaviors. These results can be given to engineers to validate and verify their design works. The proposed system can further simplify the railway system. Monitoring sensors can be set up at important places such as turnouts, immovable sections, the curved sections of embankments, and bridge intersections, reducing the cost compared to setting up sensors along the whole rail. And this system can be upgraded by installing other FBG type accelerometer to detect the wheel/rail interface response in the future for the operational condition monitoring.

References

Chang, C.-L. (2004). "Theory and practice of continuous welded rails—Use Nan Kong Shi Railway Bridge of Taichung main line for example." *J. Taiwan Railway*, 318, 53–72.

Damljanovic, V., and Weaver, R. L. (2005). "Laser vibrometry technique for measurement of contained stress in railroad rail." *J. Sound Vib.*, 282(1–2), 341–366.

Kish, A., and Coltman, M. (1990). "New techniques for rail longitudinal force measurement and rail restraint capacity evaluations." *AREA Bulletin 727*, 236–240.

Kish, A., and Samavedam, G. (1991). "Dynamic buckling of CWR track: Theory, tests, and safety concepts." *Transportation Research Record 1289*, Transportation Research Board, Washington, DC.

Kish, A., and Samavedam, G. (1999). "Risk analysis based CWR track buckling safety evaluations." *Proc., The Int. Conf. on Innovations in the Design & Assessment of Railway Track*, Delft Univ. of Technology, The Netherlands.

Lo, C. C. H., Paulsen, J. A., Kinser, E. R., and Jiles, D. C. (2004). "Quantitative evaluation of stress distribution in magnetic material by Barkhausen effect and magnetic hysteresis measurement." *IEEE Trans. Magn.*, 40(4), 2173–2175.

Matsumoto, N., and Asanuma, K. (2007). "Some experiences on track-bridge interaction in JAPAN." *Proc., Track-Bridge Interaction on High-Speed Railways Conf.*, Taylor & Francis, Porto, Portugal.

Reis, A. J., Lopes, N. T., and Ribeiro, D. (2007). "Track-structure interaction in long railway bridges." *Proc., Track-Bridge Interaction on High-Speed Railways Conf.*, Taylor & Francis, Porto, Portugal.

Szelazek, J. (1998). "Monitoring of thermal stresses in continuously welded rails with ultrasonic technique." *NDTnet*, 3(6), 1–8.

Sato, Y. (2001). *New Railroad Track Mechanics*, Chinese Railroad, ISBN 7-113-04313-5, in Chinese and Japan.

Sussmann, T., Kish, A., and Trosino, M. (2003). "Influence of track maintenance on lateral resistance of concrete-tie track." *Transportation Research Record 1825*, Transportation Research Board, Washington, DC.

Tam, H.-Y., and Ho, S.-L. (2007). "Futuristic railway condition monitoring system using photonic sensors." *Proc., The 5th National Workshop on Nondestructive Evaluation of Civil Infrastructure System*, Chinese Institute of Civil and Hydraulic Engineering, Taipei, Taiwan, 110–121.

Wegner, A. (2005). "Non-destructive determination of the stress free temperature in CWR tracks." *Proc., Int. Longitudinal Force Workshop*, Montané Comunicación, S. L., Pueblo, CO, 173–216.

Wang, C.-Y., Wang, H.-L., and Chen, M.-H. (2005). "Applications of FBG sensors on bridge health monitoring & diagnosis." *Proc., The 5th Int. Workshop on Structural Health Monitoring*, Standford Univ., Stanford, CA.